PLOS ONE

A Microscale Model for Combined CO_2 Diffusion and Photosynthesis in Leaves

Quang Tri Ho[1], Pieter Verboven[1], Xinyou Yin[2], Paul C. Struik[2], Bart M. Nicolaï[1]*

1 Flanders Center of Postharvest Technology/BIOSYST-MeBioS, Katholieke Universiteit Leuven, Leuven, Belgium, 2 Centre for Crop Systems Analysis, Wageningen University, Wageningen, The Netherlands

Abstract

Transport of CO_2 in leaves was investigated by combining a 2-D, microscale CO_2 transport model with photosynthesis kinetics in wheat (*Triticum aestivum* L.) leaves. The biophysical microscale model for gas exchange featured an accurate geometric representation of the actual 2-D leaf tissue microstructure and accounted for diffusive mass exchange of CO_2. The resulting gas transport equations were coupled to the biochemical Farquhar-von Caemmerer-Berry model for photosynthesis. The combined model was evaluated using gas exchange and chlorophyll fluorescence measurements on wheat leaves. In general a good agreement between model predictions and measurements was obtained, but a discrepancy was observed for the mesophyll conductance at high CO_2 levels and low irradiance levels. This may indicate that some physiological processes related to photosynthesis are not incorporated in the model. The model provided detailed insight into the mechanisms of gas exchange and the effects of changes in ambient CO_2 concentration or photon flux density on stomatal and mesophyll conductance. It represents an important step forward to study CO_2 diffusion coupled to photosynthesis at the leaf tissue level, taking into account the leaf's actual microstructure.

Introduction

Photosynthesis is amongst the most important metabolic processes in plants. During photosynthesis, CO_2 diffuses from the atmosphere into the leaf and finally to the site of carboxylation in the chloroplast stroma [1]. There is increasing evidence that diffusive resistances in the leaf are a limiting factor for photosynthesis [2,3].

Fick's first law of diffusion has been used to describe the net CO_2 flux from the external environment through the intercellular space towards the cells [4,5]. It postulates that gas moves from places of high concentration to places of low concentration with a rate proportional to the gradient in concentration. The stomatal conductance (g_s) determines the gas exchange from the phyllosphere into the intercellular air space. The stomatal conductance for CO_2 has been estimated based on the water vapour release from the leaf given the fact that water and CO_2 share the same gaseous diffusion pathway [6,7]. The mesophyll conductance (g_m) is defined as the conductance for the transfer of CO_2 from the intercellular air space (C_i) to the site of carboxylation in the mesophyll cells (C_c). Both g_s and g_m are apparent parameters rather than physical constants as they implicitly incorporate microstructural and biochemical features of the tissue, cells and organelles that are involved in the gas transport mechanism.

Several methods have been developed to estimate g_m. The most common method is to use a combination of gas exchange and chlorophyll fluorescence measurements [8,9,10,11,12]. It has been shown that g_m is sufficiently small to significantly decrease C_c, relative to C_i, thereby limiting photosynthesis [1,10,13,14,15,16,17]. Many physiological and leaf microstructural features have been found to correlate with g_m, including photosynthetic potential [13,17,18], stomatal conductance [13], and mesophyll surface area exposed to intercellular air spaces [18]. Tholen and Zhu [3] showed that the resistances of the cell wall and chloroplast envelope were the most important cellular limitations to photosynthesis. Further, in early reports (e.g., [13]) g_m was considered constant for a given leaf at a given temperature. Recent evidence, however, suggests that g_m is variable [19], and a response of g_m to CO_2 and irradiance has indeed been found, resembling the response of g_s to CO_2 and irradiance [1,17]. The kinetics of change of g_m in response to CO_2 have been demonstrated by observing the rate of change of g_m for different environmental variables, but a general mechanistic basis of the response has been difficult to formulate [2]. This might be due to the fact that Fick's first law of diffusion does not account for the spatial distribution of the gas exchange in relation to microstructural features such as cell arrangement, size or cell wall thickness. Moreover, chloroplast movement in the cytoplasm, carbonic anhydrase (CA) activity in different cellular organelles and the amount and role of cooporins in the membranes may contribute in facilitating CO_2 uptake [3,20,21,22].

Correlations of g_m with leaf microstructural properties have not always been clear [2]. One reason is probably that mostly single structural properties were considered in these studies described by simple parameters, such as leaf porosity or leaf mass per area. However, leaf microstructure is a complex assembly of cells of varying sizes and with tortuous connections, interlaced with distorted intercellular spaces that will affect the actual diffusion pathway in the leaf. Insight in the relation between these microstructural features and photosynthesis requires a detailed model that incorporates the microstructural geometry of the leaf. Microscale exchange of CO_2 in leaves has been investigated using theoretical models [23,24]. In these studies, tissue models were constructed by means of basic geometrical elements such as spheres and cylinders. However, these models were relatively crude compared to the actual irregular microstructure of the tissue. Also, they did not take into account the exchange barriers of biological membranes which recently were shown to be important [25]. Tholen and Zhu [3] very recently developed a 3-D model for gas transport in a single generic C_3 mesophyll cell. The model incorporated reaction diffusion equations for CO_2 and HCO_3^- and included all cellular microstructural features of the CO_2 transport pathway and associated reactions. However, being a model for CO_2 transport within a single cell, it does not consider potential resistances within the intercellular space and, more importantly, any additional resistances due to cells being attached to each other and possibly reducing the exchange surface for CO_2 considerably.

Recently, a mathematical microscale gas exchange model was developed to describe gas movements in fruit tissue through the intercellular space and cells by the authors [26,27]. The gas exchange model was based on the actual microscale geometry of the fruit tissue and accounted for both gas diffusion as well as respiration kinetics. The model was used to evaluate the effect of ambient conditions, fruit size and maturity on the intracellular O_2 and CO_2 concentrations in fruit in relation to the occurrence of anaerobis via *in silico* analysis [27,28]. In principle this model could also be used to describe microscale gas exchange in leaf tissue if the rate equations for leaf photosynthesis would be incorporated. The latter have been constructed by Farquhar, von Caemmerer and Berry [29] – the so-called FvCB model – which has been widely used for describing C_3 photosynthesis. This biochemical model has also been coupled to a simple (lumped) CO_2 exchange model [30,31,32,33]. Yin et al. [17] have recently shown how to use combined measurements of gas exchange and chlorophyll fluorescence to estimate parameters of the FvCB model.

The objectives of this article were (i) to develop a microscale model for CO_2 exchange through the leaf by coupling a detailed biophysical model of gas diffusion that incorporates the actual microstructure of the leaf to the biochemical FvCB model of photosynthesis; (ii) to validate the model with independent data, (iii) to quantify the importance of the different pathways of gas exchange; and (iv) to analyze the response of g_m and g_s to environmental factors such as CO_2 and irradiance. Wheat (*Triticum aestivum* L.) leaf was chosen as a model system.

Results

Microscopic gas concentration distribution

Mesophyll tissue contains a loose arrangement of cells in a large intercellular space. However, cells inevitably touch each other, thereby reducing the gas exchange surface area and introducing an additional, local resistance to CO_2 transport. This would translate into local CO_2 concentration gradients. We decided to carry out some simulations to test this hypothesis with a microscale model that combines a diffusion model for CO_2 and HCO_3^- with the FvCB model for CO_2 fixation in the chloroplasts and incorporates the actual 2-D leaf tissue microstructure.

The CO_2 distribution computed by the microscale model for the wheat leaf corresponding to ambient conditions of 350 µmol mol^{-1} CO_2, 21% O_2, 1000 µmol m^{-2} s^{-1} I_{inc} and 25°C is shown in Figure 1. The meaning and units of all symbols are given in Table 1. As expected, the CO_2 concentration in the pores is considerably higher than inside the mesophyll cells. However, the concentration in the intercellular space is definitely not uniform, probably due to the relatively compact mesophyll tissue microstructure of wheat leaves compared to that of other species. Further, relatively large CO_2 gradients can be observed within cell clusters. For this particular mesophyll tissue, the resistance to CO_2 transport is clearly not negligible.

A detailed analysis of the calculated resistances of the different compartments of the leaf tissue is shown in Table 2. The resistance of the chloroplast envelope contributed up to 11.43% of the total resistance. This suggests that the chloroplast envelope effectively contributes significantly to the resistance to CO_2 transport in the mesophyll cells, confirming the simulation results of Tholen and Zhu [3] for single mesophyll cells. Microscale simulations with a lumped intracellular compartment (without distinguishing the individual chloroplasts or other organelles) have been additionally carried out (Text S1, Figure S1). These results showed that there was a good similarity in total gas flux between the lumped model and the one with the chloroplasts taken into account the resistance of the chloroplast envelope; the latter, however, predicted a g_m that was 12.7% higher than that obtained with the lumped intracellular model. Apparently, the reduced resistance to CO_2 transport due to the position of the chloroplasts near the plasma membrane outweighs the increased resistance due to the double membrane of the chloroplasts compared to the lumped model. The modelled distribution of $V_{c,max}$ along the depth of a typical leaf is shown in Figure 2. There is a decreasing trend at the abaxial side of the leaf. Also, there is a dip where there is a vascular bundle.

Photosynthesis in response to CO_2 concentration and model validation

In a next step, we investigated whether the microscale model was able to predict the measured response of leaf photosynthesis to the ambient CO_2 concentration in photorespiration conditions. The following convention for symbols is used further: macroscopic variables which were estimated from gas exchange and chlorophyll fluorescence experiments are denoted by a '^' symbol. Volume averaged variables calculated from the microscale model are overlined (see more details in Materials and Method section).

Plots of the measured and simulated net photosynthesis rate at C_i values from 50 to 1500 µmol mol^{-1} at 1000 µmol m^{-2} s^{-1} I_{inc} and 21% O_2 are shown in Figure 3. A good agreement was found between measured and simulated data. $\hat{A}$ rapidly increased at low $\hat{C_i}$ concentrations but saturated at high CO_2 concentrations (Figures 3A&3B). The relationship between $\hat{C}_c$ and $\overline{C}_c$ is shown in Figures 3C&3D. They are approximately equal at low CO_2 concentrations (<500 µmol mol^{-1}), but at high CO_2 concentrations $\hat{C}_c$ levels off. In Figures 3E & 3F, g_m is plotted as a function of C_i. Excluding the low-CO_2 region where any assessment of g_m is uncertain [1,2], clearly $\hat{g}_m$ decreased with increasing CO_2 levels; $\overline{g}_m$ also decreased with increasing CO_2 levels but then stabilized at high CO_2 concentrations. Similar results were found when validating the model using data obtained from wheat leaves at 2 weeks after flowering (Figure S2).
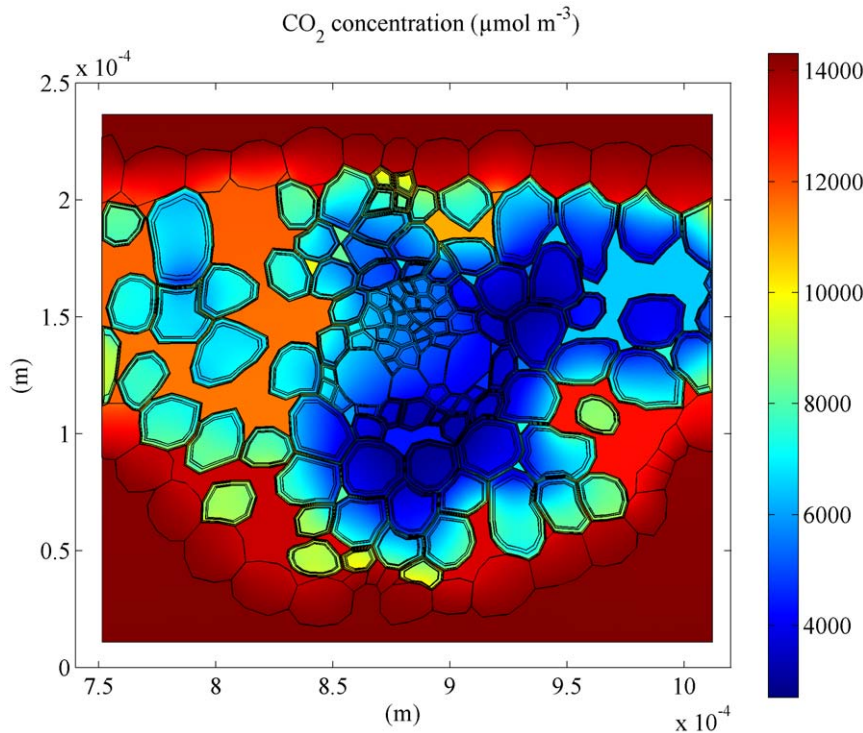
Figure 1. Computed CO₂ distribution in wheat leaf. The ambient conditions were 350 µmol mol^{-1} CO$_2$, 21% O$_2$, I_{inc} = 1000 µmol m^{-2} s^{-1} and T_{leaf} = 25°C. Concentrations are expressed in µmol m^{-3}.
doi:10.1371/journal.pone.0048376.g001

We then validated the microscale model using data obtained at 2% O$_2$. The computed CO$_2$ assimilation rate was slightly underestimated compared to the measurements (Figure 4), especially for the condition of high and low N supply at flowering stage (Figures 4A&4B).

Photosynthesis in response to irradiance

Yin et al. [17] found that g_m and g_s increase with increasing I_{inc}. We wanted to evaluate whether the microscale model indeed predicts such behaviour. Microscale gas exchange simulations were carried out for different values of I_{inc} increasing from 0 to 2000 µmol m^{-2} s^{-1} (350 µmol mol^{-1} C_a and 21% O$_2$). If using a constant D_{epi} = 1.67×10^{-7} m^2 s^{-1} (Table 3), the CO$_2$ concentration in the intercellular space was overestimated by the model for the conditions of low light intensity (results not shown). As D_{epi} was considered in the microscale model as a lumped parameter that included the gas diffusion through the stomata, its value was expected to vary with irradiance. The high N data at flowering stage were used for fitting $\bar{g}_s$ to $\hat{g}_s$ and to determine D_{epi}. The effects of light on D_{epi} and g_s are shown in Figure 5. The results confirm that D_{epi} and g_s increase with I_{inc}, due to the opening of the stomata by light [34].

The $\bar{C}_c$ values were larger than the measured ones at low I_{inc} while at high values of I_{inc} both C_i and C_c in the model and measurement levelled off (Figures 6A&6B). $\bar{A}$ as a function of I_{inc} agreed well with the measured values at low I_{inc} but was underestimated at high I_{inc} (Figures 6C&6D). While $\hat{g}_m$ seemed to be very sensitive at low I_{inc}, $\bar{g}_m$ was not (Figures 6E&6F). Similar results were found for validation on wheat leaf at 2 weeks after flowering (Figure S3). Overestimations of $\bar{C}_i$ and $\bar{C}_c$ compared to the measurements were found. Note that the $\hat{g}_s$ obtained for two weeks after flowering was lower than the $\hat{g}_s$ at the flowering stage,

while the values of D_{epi} at different I_{inc} applied in the simulation resulted in $\bar{g}_s$ similar to $\hat{g}_s$ for the high N leaves at flowering stage.

Microstructure effect on mesophyll conductance

The anatomy of the leaf may have an effect on microscale gas exchange and result in variation in mesophyll conductance. In order to test this hypothesis, the mesophyll conductance was computed for four different micro-structures of a wheat leaf based on light microscopic images at 15, 30, 60 and 90 mm above the leaf base taken from the literature [35]. Simulations were carried out at different values of C_a from 50 to 1500 µmol mol^{-1}, I_{inc} = 1000 µmol m^{-2} s^{-1} in photorespiration conditions (21% O$_2$). In Figure 7 the computed values of $\bar{g}_m$ for four different microscale geometries are shown as a function of $\bar{C}_i$. The $\bar{g}_m$ values varied for the different microstructures, validating our hypothesis. A decreasing trend of $\bar{g}_m$ with increasing $\bar{C}_i$ was found consistently, irrespective of leaf microstructures. This is a simulation result that follows from the model and it is difficult to trace this to a particular submodel.

Discussion

CO₂ transport model

Fick's diffusion equation is applicable to transport of a chemical species such as CO$_2$ in a continuum material such as water. It can be related to Brownian motion according to the Einstein–Smoluchowski equation that has its foundations in statistical mechanics. Several authors have used the diffusion equation to describe CO$_2$ uptake by leaves [36]. Such models were solved with geometrical simplifications such as a 1D model of CO$_2$ drawdown in the leaf [37], a restricted and simplified zone analysis of diffusion from a small sub-stomatal cavity into a hemispherical

Table 1. List of model variables, their symbols and definitions.

Variable	Definition
A_G	Gross photosynthesis rate (µmol CO$_2$ m^{-2} s^{-1})
A_G^*	Gross volumetric photosynthesis rate of chloroplast (µmol CO$_2$ m^{-3} s^{-1})
$\hat{A}$	Measured net photosynthesis rate (µmol CO$_2$ m^{-2} s^{-1})
$\overline{A}$	Mean net photosynthesis rate computed from microscale model (µmol CO$_2$ m^{-2} s^{-1})
B	Net hydration of CO$_2$ to HCO$_3^-$ (mol m^{-3} s^{-1})
C_a	Ambient air CO$_2$ concentration (µmol mol^{-1})
C_c	Mesophyll CO$_2$ concentration (µmol mol^{-1})
$C_{HCO_3^-,c}$	HCO$_3^-$ concentration of the mesophyll (mol m^{-3})
C_i	Intercellular CO$_2$ concentration (µmol mol^{-1})
C_j	CO$_2$ concentration in phase j
$\hat{C}_c$	Measured mesophyll CO$_2$ concentration using combined gas exchange and chlorophyll fluorescence measurements (µmol mol^{-1})
$\hat{C}_i$	Measured intercellular CO$_2$ concentration (µmol mol^{-1})
$\overline{C}_c$	Mean mesophyll CO$_2$ concentration computed from microscale model (µmol mol^{-1})
$\overline{C}_i$	Mean intercellular CO$_2$ concentration computed from microscale model (µmol mol^{-1})
D_j	Diffusivity of phase j (m^2 s^{-1})
D_c	Diffusivity of CO$_2$ in the mesophyll cytoplasm (m^2 s^{-1})
D_{epi}	CO$_2$ diffusivity of epidermis layer (m^2 s^{-1})
D_w	CO$_2$ diffusivity of cell wall (m^2 s^{-1})
$D_{HCO_3^-,c}$	Diffusivity of HCO$_3^-$ in the mesophyll cytoplasm (m^2 s^{-1})
d	Average thickness of tissue (m)
f_c	The fraction of chloroplasts of the leaf
f_m	The fraction of cytosols of the leaf
g_s	Stomatal conductance (mol m^{-2} s^{-1})
g_m	Mesophyll conductance (mol m^{-2} s^{-1})
$\hat{g}_m$	Measured mesophyll conductance using combined gas exchange and chlorophyll fluorescence measurements (mol m^{-2} s^{-1})
$\overline{g}_m$	Computed mesophyll conductance from Eq. 14 (mol m^{-2} s^{-1})
H	Henry's constant for CO$_2$ (mol m^{-3} liquid) (mol m^{-3} gas)$^{-1}$
$[H^+]$	H$^+$ concentration (mol L^{-1})
I_{inc}	Photon flux density incident to leaves (µmol photon m^{-2} s^{-1})
J	Rate of potential electron transport calculated from chlorophyll fluorescence measurements (µmol electron m^{-2} s^{-1})
k_1	CO$_2$ hydration velocity constant (s^{-1})
k_2	CO$_2$ dehydration velocity constant (s^{-1})
K	Acid dissociation constant for H$_2$CO$_3$ (mol L^{-1})
$K_{m,C}$	Michaelis-Menten constant of Rubisco for CO$_2$ (µmol mol^{-1} or µbar)
K_{m,O_2}	Michaelis-Menten constant of Rubisco for O$_2$ (mbar)
O_2	Oxygen partial pressure (mbar)
P_m	CO$_2$ permeability of cell membrane (m s^{-1})
R	Universal gas constant (8.314 J mol^{-1} K^{-1})
R_d	Day respiration (i.e. respiratory CO$_2$ release other than by photorespiration) (µmol CO$_2$ m^{-2} s^{-1})
R_d^*	Volumetric respiration rate (µmol CO$_2$ m^{-3} s^{-1})

Table 1. Cont.

Variable	Definition
s	Slope factor for converting chlorophyll fluorescence-based PSII electron efficiency into J (−)
$S_{c/o}$	Relative CO$_2$/O$_2$ specificity factor for Rubisco (mbar µbar^{-1})
T_{leaf}	Temperature of the leaf (K)
T_p	Rate of triose phosphate export from the chloroplast (µmol m^{-2} s^{-1})
t	Time (s)
V_m	Total mesophyll cells volume (m^3)
$V_{c,max}$	Maximum rate of Rubisco activity-limited carboxylation (µmol m^{-2} s^{-1})
$V_{c,max}(y)$	The relative photosynthetic capacity at a depth y inside the leaf
w_c	Rate of Rubisco activity-limited carboxylation (µmol m^{-2} s^{-1})
w_j	Rate of electron transport-limited carboxylation (µmol m^{-2} s^{-1})
w_p	Rate of TPU-limited carboxylation (µmol m^{-2} s^{-1})
$w(y)$	The width of the leaf at the depth y (m)
y	The depth of the leaf from adaxial surface (m)
ϕ	CO$_2$ flux through the membrane (µmol m^{-2} s^{-1})
Γ^*	C_c-based CO$_2$ compensation point in the absence of R_d (µmol mol^{-1} or µbar)

The unit µmol mol^{-1} for CO$_2$ concentration (often used in the FvCB model) was converted to µmol m^{-3} for use in the gas diffusion model by multiplying with a factor $P(R \cdot T)^{-1}$ for CO$_2$ concentration in the gas phase and $P \cdot H (R \cdot T)^{-1}$ for CO$_2$ concentration of the mesophyll, respectively. P (Pa) is the total pressure of the ambient air, R (J mol^{-1} K^{-1}) is the universal gas constant and T (K) is the temperature.

region surrounding it [38], and CO$_2$ diffusion through a single stoma and the surrounding mesophyll using an axial symmetry model [23]. Aalto and Juurola [24] constructed a 3-D model for CO$_2$ gas exchange through the leaf with basic geometrical elements such as spheres and cylinders representing mesophyll cells. While in their model the cells were separated by air gaps, in reality cells touch each other and this contact may reduce both the surface available for CO$_2$ exchange and the diffusion among the cells as we have clearly shown. The most realistic photosynthesis model to date was recently described by Tholen and Zhu [3]. Their model, while addressing 3-D CO$_2$ transport in a single mesophyll cell and incorporating subcellular features such as chloroplasts and mitochondria, does not account for any resistances due to the leaf microstructure and in particular the mesophyll.

In our model we incorporated for the first time the actual microstructure as observed from microscopy images in the CO$_2$ transport model. We considered six materials (epidermis, cell wall, cytoplasm, chloroplast, vacuole and air) and we assumed that these materials were proper continuum materials so that we could assume Fickean diffusion of CO$_2$ within each of them. Membranes were modelled as resistances. In contrast to the model of Aalto and Juurola [24], our model does account for the effect of mesophyll cells touching each other and thereby reducing the exchange surface between mesophyll and intercellular space. Further, our simulations show that wheat leaves with different microstructure have widely different $\overline{g}_m$ values (Figure 7), indicating a clear effect of microstructure on gas transport (also see next section). This implies that our model is in principle not restricted to leaf types in which air space resistance is negligible as in the model of Tholen and Zhu [3].

Table 2. Resistance analysis of different compartments of the wheat leaf described in the model, for the CO_2 diffusion from ambient air to chloroplast stroma.

	Resistance	
	(m² s mol⁻¹)	(%)
Epidermis	1.38	16.89
Intercellular space	2.54	31.10
Cell wall	1.89	23.05
Plasma membrane	0.44	5.37
Cytosol	0.52	6.38
Chloroplast envelope	0.94	11.43
Stroma	0.47	5.78
Total	8.18	100.00

The resistances were calculated by dividing the average concentration difference across compartments by the average flux expressed per unit of exposed leaf surface.
doi:10.1371/journal.pone.0048376.t002

We carried out a simulation in which we replaced air by helox in the model, corresponding to an increase of the diffusivity of CO_2 in the gas phase by 2.33 compared to that of the original model. At ambient conditions of 350 μmol mol⁻¹ CO_2, 21% O_2, $I_{inc} = 1000$ μmol m⁻² s⁻¹ and 25°C, A was 6.8% higher than in the case of the air. This corresponds to the results of Parkhurst and Mott [38] who experimentally found that A was up to 7% higher in the amphistomatous leaves compared to air and up to 27% higher for the hypostomatous ones. While we did not do any measurements with helox, this result provides additional evidence that our model predicts realistic results. Additionally, it indicates that the intercellular space affects CO_2 transport and thus photosynthesis. Note that a lumped model, in contrast, cannot explain the effect of helox on photosynthesis

The effect of nitrogen treatment on the photosynthetic parameters of wheat leaves at different development stages was investigated by Yin et al. [17]. A relatively small effect of nitrogen treatment could be observed in the flowering stage; two weeks after flowering the effect was somewhat larger (Figures 3, 6; Figure S2
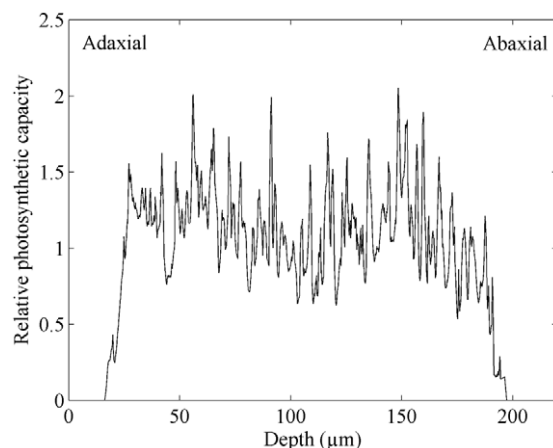
Figure 2. Distribution of the relative photosynthetic capacity along the depth of the wheat leaf computed from the modelled microscale geometry.
doi:10.1371/journal.pone.0048376.g002

and S3). The effect of development stage was, however, considerable (Figures 3, 6; Figure S2 and S3). The more significant difference in the later stage was probably due to the greater difference in the content of leaf nitrogen as large amount of leaf nitrogen was translocated into grains during grain filling.

We calibrated and validated the model at one temperature (25°C), as data were available for this temperature only [17]. However, temperature is known to have a large effect on photosynthesis [39,40,41,42]. The temperature dependence of physical constants such as the solubility and diffusivity of CO_2 and HCO_3^- is known [44]. Also, mathematical expressions have been developed to describe the temperature dependence of the parameters of the FvCB model for different species [39,40,41], but not for wheat. In fact, the values of the activation energy of $V_{c,max}$ and J_{max} used by De Pury and Farquhar [43] and Archontoulis et al. [43] for wheat were actually obtained by Badger and Collatz [44] from experiments with *Atriplex glabriuscular* leaf and by Farquhar et al. [29]. Preliminary simulations with temperature dependent $V_{c,max}$ and J_{max} values taken from these references showed that the net photosynthesis of wheat leaves is highly dependent on temperature (Figure S4). Additional experiments are required to determine the temperature dependence of the parameters of the photosynthesis kinetics of wheat.

In our model it is assumed that CO_2 transport in the cell occurs mainly in the form of CO_2 and HCO_3^- depending on the local pH. The dissociation of HCO_3^- to H^+ and CO_3^{2-} is not significant at pH values below 8. There is both theoretical and experimental evidence for significant carbonic anhydrase (CA) dependent facilitation of CO_2 transport in C_3 plants [20,22,45]. CA isozymes may be active in different cellular components [22,46] and may affect CO_2 transport. In fact, Tholen and Zhu [3] calculated that removing all CA from the stroma would reduce g_m by 44%. As little information is available about the rate constants of the hydration and dehydration of CO_2 by CA, or its activity in the different organelles of the cell, we decided at this stage to not include CA activity in the microscale model until more information would become available; incorporation in the model would be straightforward and desirable, though.

The value of P_m was taken from Evans et al. [20] and Tholen and Zhu [3], who used the results of Gutknecht et al. [47] from experiments with equimolar mixtures of egg lecithin and cholesterol. The chemical composition of such a bilayer is, however, likely to be different from that of the cellular membranes of wheat leaf. The permeability of both the plasma and chloroplast membrane has also been shown to depend on the amount of embedded aquaporins (cooporins) [25]. In fact, Evans et al. [20] found values for P_m ranging from 10^{-6} to 1.6×10^{-2} m s⁻¹ in the literature. When we used the value reported by Uehlein et al. [25] ($P_m = 0.8 \times 10^{-6}$ m s⁻¹) we obtained a value of $\overline{g}_m$ that was considerably smaller than the measured one. More research on cell membrane permeability of plants and wheat in particular is thus required.

The microscale model described here does not consider the light profile inside the leaf yet. Coupling a full light penetration model to this model may be very helpful to estimate the distribution of quanta that are absorbed by the mesophyll cells within the leaf for photosynthesis. Future research thus should also address models for light propagation in leaf tissue.

Effect of leaf microstructure on CO_2 diffusion

During photosynthesis, CO_2 moves from the atmosphere surrounding the leaf to the sub-stomatal internal cavities through stomata, and from there to the site of carboxylation inside the mesophyll cells. The simulation results indicated that gas exchange
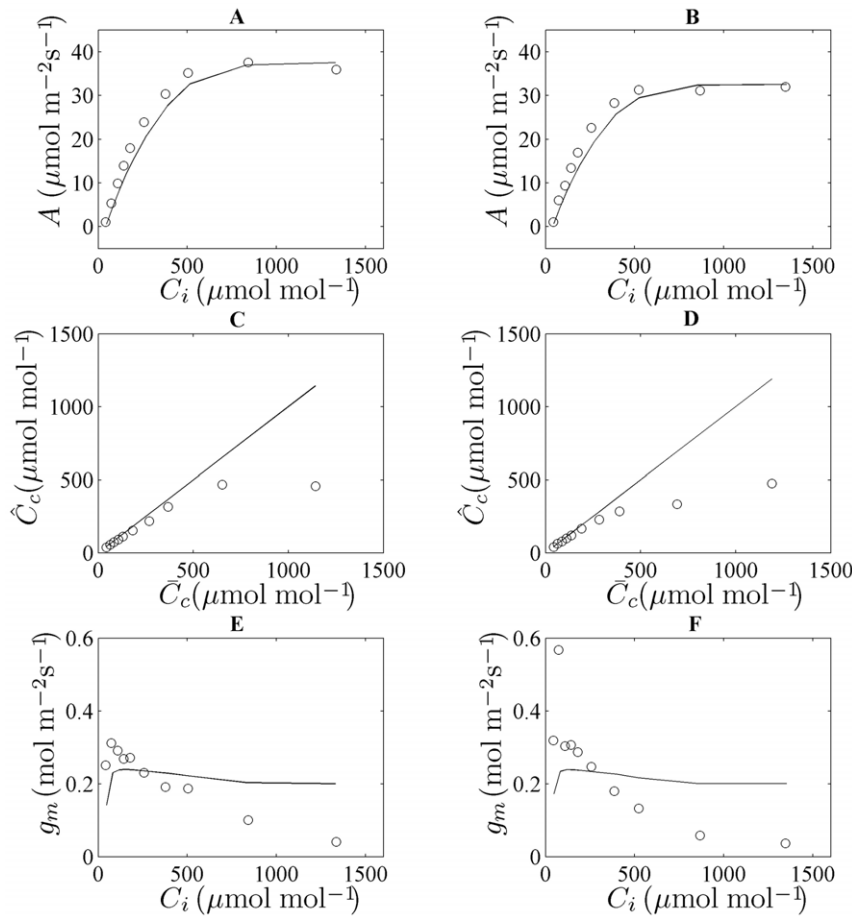
Figure 3. Simulations and measurements at different conditions of C_i **at 21% O$_2$,** I_{inc} **= 1000 µmol m^{-2} s^{-1} and 25°C at flowering stage.** Figures (A) and (B) show A as function of C_i for the flag leaves at high and low N supply, respectively. The symbols represent measurements ($\hat{A}$ versus $\hat{C}_i$) while the lines indicate model predictions ($\overline{A}$ versus $\overline{C}_i$). Figures (C) and (D) depict $\hat{C}_c$ versus $\overline{C}_c$ for high and low N supply flag leaves, respectively. The diagonal lines indicate perfect correspondence. Figures (E) and (F) show g_m as function of C_i for high and low N supply flag leaves, respectively. The solid (—) line represents $\overline{g}_m$ versus $\overline{C}_i$. The symbols (o) represent the measured data ($\hat{g}_m$ versus $\hat{C}_i$). Data are from Yin et al.[17].
doi:10.1371/journal.pone.0048376.g003

through the microstructure is very heterogeneous. Large gradients and low CO$_2$ concentrations were mainly found inside the mesophyll cells and cell clusters due to photosynthesis and limited diffusion of CO$_2$ in the mesophyll cells. The CO$_2$ concentration at the carboxylation site in the chloroplast stroma, C_c, in C$_3$ plants is lower than C_i [3,11,48,49]. The diffusion barriers such as the water-filled pores of the cell wall, plasma membrane, cytosol, the envelope and stroma are responsible for the resistance of CO$_2$ along the pathway from intercellular space to stroma [20]. Several authors (Evans and von Caemmerer [11], Evans et al. [14], Evans et al. [20], Terashima et al. [49]) reported that chloroplasts adhere exclusively to the plasmamembrane of mesophyll cells and, therefore, path length of CO$_2$ transport over the cytoplasm is reduced. Tholen et al. [21] indicated the possibility of chloroplast movement that may have significant consequences for the diffusion of CO$_2$ through the mesophyll. Simulations with a microscale model with chloroplasts lumped over the mesophyll cells showed that the predicted value of g_m was lower than when they incorporated chloroplasts near to the cell wall. This indicates that the position of the chloroplasts next to the plasma membrane does indeed reduce the resistance for CO$_2$ transport.

The distribution of $V_{c,max}$ depends on the distribution of chlorophyll through the leaf and the presence of the vascular region. In *Eucalyptus pauciflora* leaves, the photosynthesis capacity has been shown to be low in the vascular bundle region [50]. Evans and Vogelmann [51] showed that with increasing depth the photosynthetic capacity first increased followed by a strong decrease which finally levelled off in spinach leaves. This was not implemented in our model as there was no data available for wheat.

Early literature has assumed that simple diffusion through cellular membranes [52] and/or leaf structural features [14,53,54] are responsible for most of the variation in g_m. Flexas et al. [2] supposed that g_m can be correlated to some leaf microstructural features. Our simulation results provided even more direct evidence of gas concentration gradients in relation to the microstructure topology of leaves and the effect of variation of the leaf microstructure on g_m: depending on the value of $\overline{C}_i$, the value of $\overline{g}_m$ that was computed for different microstructure topologies was 30% different from the mean value (Figure 7). Biological variation thus considerably affects the mesophyll conductance. This may depend on the species, though: the microstructure of wheat leaf mesophyll is relatively tight compared to that of other species. Future photosynthesis models should thus not simply ignore the tissue microstructure.
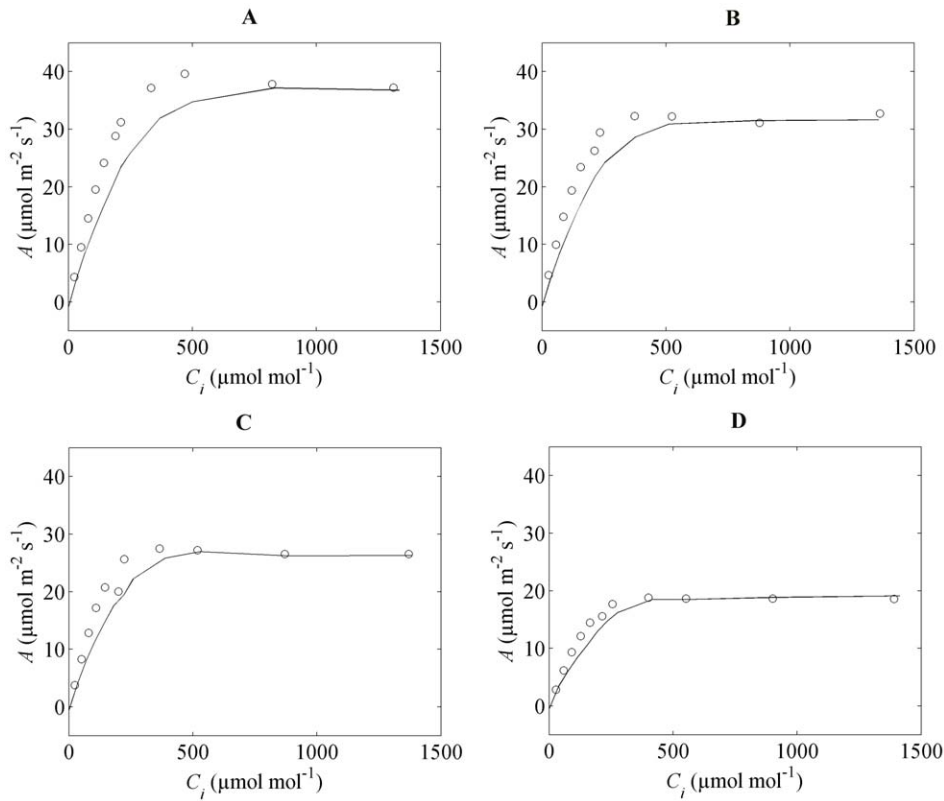
Figure 4. CO₂ response of net CO₂ assimilation rates of the flag leaves under the conditions of 2% O₂. (A) and (B) correspond to flag leaves at high N and low N supply at flowering while (C) and (D)correspond to flag leaves at high N and low N supply at two weeks after flowering. The symbols represent the measured values of versus $\widehat{C}_i$ [17]; the solid (—) represent the computed $\overline{A}$ versus $\overline{C}_i$.
doi:10.1371/journal.pone.0048376.g004

Table 3. Physical parameters of the microscale gas exchange model.

Model parameters	Symbol	Values
Diffusivity		
- Pore	$D_{CO_2,g}$	1.60×10^{-5} m² s⁻¹ at 20°C[a]
- Cytosol and stroma	$D_{CO_2,l}$	1.67×10^{-9} m² s⁻¹ at 20°C[a]
- Cell wall	D_w	3.437×10^{-7} m² s⁻¹
- Epidermis	D_{epi}	1.672×10^{-7} m² s⁻¹
	$D_{HCO_3^-,c}$	1.17×10^{-9} m² s⁻¹[b]
Cell wall thickness	L_w	0.5 µm
Membrane permeability	P_m	3.5×10^{-3} m s⁻¹[c]
Henry's constant	H	0.83 (mol m⁻³ liquid) (mol m⁻³ gas)⁻¹ at 25°C[a]
CO₂ reaction rate constants	k_1	0.039 s⁻¹[d]
	k_2	23 s⁻¹[d]
	K	2.5×10^{-4} mol L⁻¹[d]

[a]Lide [43],
[b]Geers and Gros [76],
[c]Gutknecht et al. [47],
[d]Jolly [77].
Symbols are defined in the Table 1.
doi:10.1371/journal.pone.0048376.t003

The epidermis was implemented as a homogeneous layer without explicitly modelling the stomata, resulting in a high value of D_{epi}. The positive dependence of D_{epi} on I_{inc} (Fig. 6) is most probably due to the aperture of the stomata in response to the light. The cell walls were modelled as channels connecting the larger pores in the tissue, thereby creating a void network structure that facilitates gas exchange resulting in a high diffusivity of cell wall (D_w). When the cell wall structure was assumed to be saturated with liquid in the 2D model, the net CO₂ assimilation flux decreased drastically compared to the measurement and resulted in a significant underestimation of mesophyll CO₂ concentration. Evans et al. [20] showed that CO₂ diffusivity of the cell wall (1.7×10^{-9} m⁻² s⁻¹) was much smaller than the value obtained here (see Table 3). As *in vivo* the cell walls are expected to be fully hydrated, this may indicate that the interconnectivity of the microstructure is considerably larger than expected from the 2-D microscale geometry. Consequently, D_w is in our model an apparent parameter that accounts for both CO₂ diffusion in the cell wall but also for the connectivity of the intercellular space in 3-D. Lateral gas diffusion within the intercellular air space has been studied by Pieruschka et al. [55] and Morison et al. [56]. Morison et al. [57] indicated that the supply of CO₂ from nearby stomata usually dominates assimilation, but that lateral supply over small distances can be important if stomata are blocked, particularly when the assimilation rate is low. The discrete positions of stomata may thus have an influence on the diffusion gradients in the leaf. As the 2-D model described here cannot fully capture gas transport through and from discrete stomata, a 3-D microscale gas transport simulation in a real leaf geometry is required to
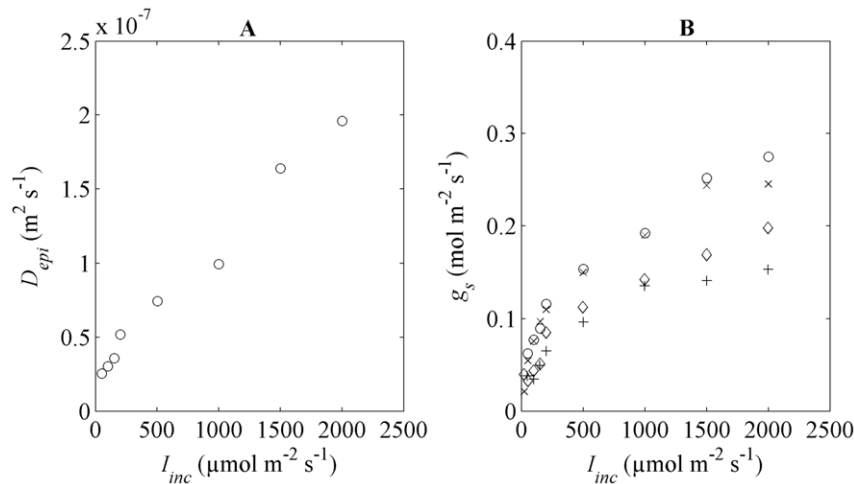
Figure 5. Epidermal diffusion and CO₂ stomatal conductance as function of I_{inc}. (A) Fitted epidermal diffusion (D_{epi}) as function of I_{inc}. (B) Measured CO₂ stomatal conductance (g_s) as a function of I_{inc}. The symbols (o) and (×) represent high and low N supply flag leaves at flowering stage, respectively while symbols (◇) and (+) represent high and low N supply flag leaves at two weeks after flowering.
doi:10.1371/journal.pone.0048376.g005

understand lateral gas diffusion in the leaves. A 3-D network structure with strong connectivity has indeed been observed in several plant tissues such as fruits [58,59,60]. The 3-D microstructure of stomatal aperture and the corresponding microscale gas exchange through the stomata have recently been investigated using a diffusional resistance model [61]. Indeed, the 2-D gas exchange model described here is an important step toward a realistic full 3-D gas exchange model based on 3-D microstructure of leaf tissue which has not been achieved so far. The extension of our model to a 3-D model requires the geometrical model to be changed from 2-D to 3-D which is not trivial and requires advanced 3-D visualisation techniques such as synchrotron X-ray micro computed tomography [60]. The model equations, however, do not need to be changed.

It is important to note that our microstructural model (and a possible 3-D extension) complements rather than replaces the lumped approach for photosynthesis modelling that has been used by many authors [1,5,10,11,12]. A lumped model, even when it fits GE/CF measurements very well, does not improve our understanding on the role of mesophyll porosity, cell size, presence of vascular bundle or any other microstructural features on photosynthesis. Our 2-D model (and a future 3-D even more) does provide such information.

Effect of CO₂ and irradiance on mesophyll conductance

We confronted our model extensively with measured gas exchange and chlorophyll fluorescence data and obtained in general a good agreement between simulated and measured values. However, the model failed to predict the decrease of $\hat{g}_m$ at high CO₂ values that was seen in the measurements and that is a topic of current debate [1,17].

One explanation for this mismatch could be the uncertainty on the estimation of $\hat{g}_m$ based on combined gas exchange and chlorophyll fluorescence measurements, and the estimation of Harley et al. [10], Yin and Struik [12]. The latter authors found that the estimated mesophyll conductance becomes increasingly sensitive to variations of the measurements as the value of g_m increases, and can be affected by both statistical artifacts in curve fitting and biological uncertainties in thylakoid stoichiometry [12]. In addition, Evans [62] and Terashima et al. [63] indicated that electron transport rates calculated from chlorophyll fluorescence

may have potential errors, which the calibration procedure based on Equation (12) may not account for sufficiently. This would also explain the mismatch between $\hat{C}_c$ and $\overline{C}_c$ as observed in Figures 3C and 3D. However, the large discrepancy between $\hat{g}_m$ and $\overline{g}_m$ appears already at intermediate levels of C_i, and is thus not well explained by these considerations. Another, more plausible, explanation may be that there are effects that have not been incorporated in our model. For example, Tholen and Zhu [3] used a gas transport model for single mesophyll cells to show that increasing the permeability of the chloroplast membrane for HCO_3^- would indeed explain decrease of $\hat{g}_m$ as a function of C_i. Also, transport through the chloroplast membrane may be regulated by CA: CO₂ diffuses more easily through membranes than HCO_3^-, so any regulatory mechanism that would affect the expression of CA and thus the equilibrium between CO₂ and HCO_3^- in different cellular compartments would also affect their transport through the relevant membranes. Finally, cooporins have been shown to be present in chloroplast membranes and may significantly affect membrane permeability [25]. These mechanisms may also explain the discrepancy between $\overline{g}_m$ and $\hat{g}_m$ at low I_{inc}.

Materials and Methods

Model assumptions

The following assumptions were made:

Model dimension. Gas transport is essentially 3-D. We have shown previously [60,64] that in dense tissue such as in the cortex of fruit, pores that appear unconnected in 2-D may in fact be connected when visualised using 3-D techniques such as X-ray microfocus computed tomography (μCT). The reason that we have implemented a 2-D here instead of a 3-D model is the fact that μCT – the only feasible technique for 3-D visualisation of plant tissue at this resolution – provides insufficient contrast to discriminate organelles in a cell, and, for example, locate the position of the chloroplasts to include them in the geometrical model. Moreover, the best resolution that currently can be obtained with μCT (about 500 nm) is not enough to visualise the cell wall with sufficient contrast to allow segmentation of individual cells. This is a prerequisite for the method we used to artificially position the chloroplast layer inside the cell close to the
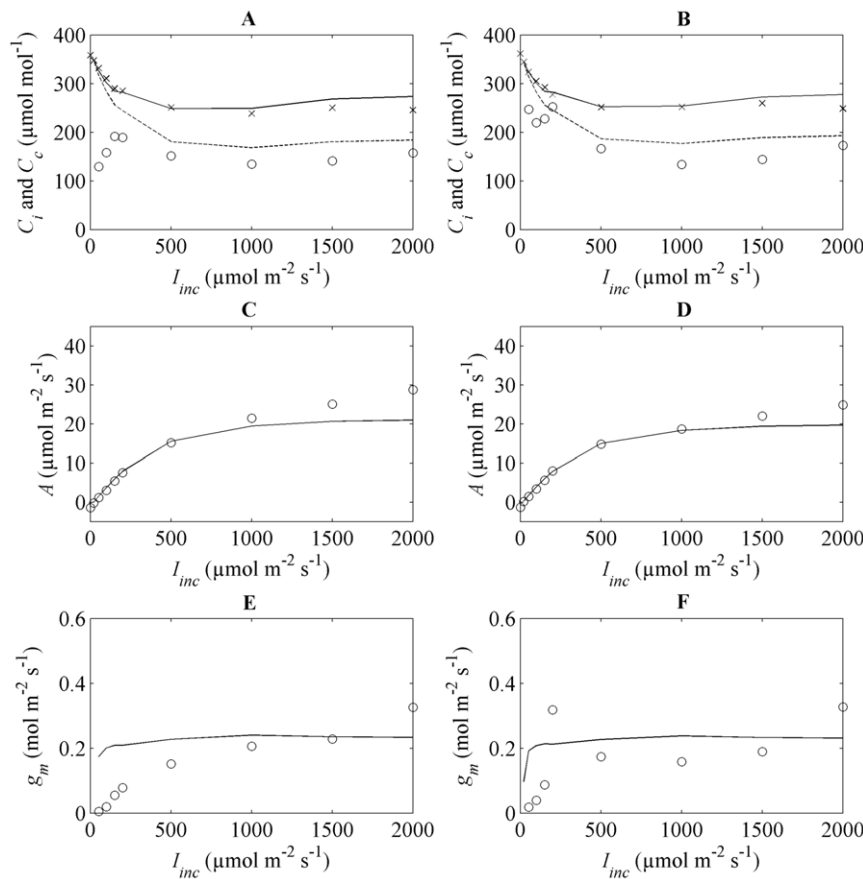
Figure 6. Model predictions (lines) versus measurements (symbols) of photosynthesis variables for 350 μmol mol^{-1} CO$_2$, 21% O$_2$, I_{inc} from 0 to 2000 μmol m^{-2} s^{-1} and 25°C at flowering stage. Left figures represent fitting results using data from high N supply flag leaves; right figures were simulations for low N supply flag leaves. Figure (A) and (B) show C_i and C_c as a function of I_{inc}; solid lines (—) and dashed lines (- -) represent $\overline{C_i}$ and $\overline{C_c}$, symbols (×) and (o) represent $\widehat{C_i}$ and $\widehat{C_c}$, respectively. Figure (C) and (D): A as function of I_{inc}. Figure (E) and (F): mesophyll conductance $\overline{g}_m$ (—) or $\hat{g}_m$ (o) as function of I_{inc}. Data from Yin et al. [17].
doi:10.1371/journal.pone.0048376.g006

plasmalemma (see further). As mesophyll is much less dense we expect that the difference between 2-D and 3-D is not as large as in fruit cortex tissue, but this remains to be investigated in future research.

Intercellular space. In contrast to the model of Tholen and Zhu [3], our model explicitly incorporated the actual microstructure of the mesophyll tissue, including the intercellular space and cells touching each other. This allows investigating any resistances these features may cause in addition to those investigated by the latter authors.

Cell organelles. Chloroplasts and mitochondria were modelled as different homogeneous layers in the cell rather than as individual organelles. This considerably reduced the complexity of the model and the required mesh density. This assumption was supported by the model of Tholen and Zhu [3] that displayed almost one dimensional gas exchange in a single isolated mesophyll cell one. It was further assumed that a mesophyll cell contained a single, large vacuole.

Stomata. In a 2-D model the real stomata distribution cannot be implemented without considerably overestimating the overall stomatal gas exchange of the leaf; only a true 3-D model would allow incorporating the stomata as such. We therefore modelled the epidermis layer as a continuum material with an effective diffusivity D_{epi}. This lumped parameter implicitly incorporates stomatal gas exchange in such a way that the overall conductance of the epidermis in the model would be equal to the measured one.

Localisation of photosynthesis. We assumed that there was no photosynthesis in the epidermis and vascular bundle. Respiration was assumed to take place in the epidermis, the cytoplasm of mesophyll cells and phloem; xylem cells were assumed not to respire. Xylem was identified as large cells in the vascular bundle facing the adaxial epidermis.

Spatial dependence of photosynthesis rate. Several authors have found a spatial dependence of the photosynthesis rate [51,65,66]. The rate of photosynthesis across a leaf is determined by the light absorption profile and the profile of the photosynthetic capacity. With increasing depth the photosynthetic capacity first increases followed by a strong decrease and finally levels off. Although we realise that this would affect the modelling results, we did not find sufficient quantitative data on the spatial dependence of the photosynthesis rate in wheat.

Light transport. As light penetrates the leaf it is absorbed by the photosynthetic pigments and scattered at air-water interfaces. Palisade cells facilitate the penetration of collimated light into the inner parts of the leaf, whereas the spongy mesophyll scatters the light thus increasing the probability of the light being absorbed. Because of the difficulty of modelling of this process (for example by means of Monte Carlo methods) we have assumed here that the photon flux density is uniform in the leaf.
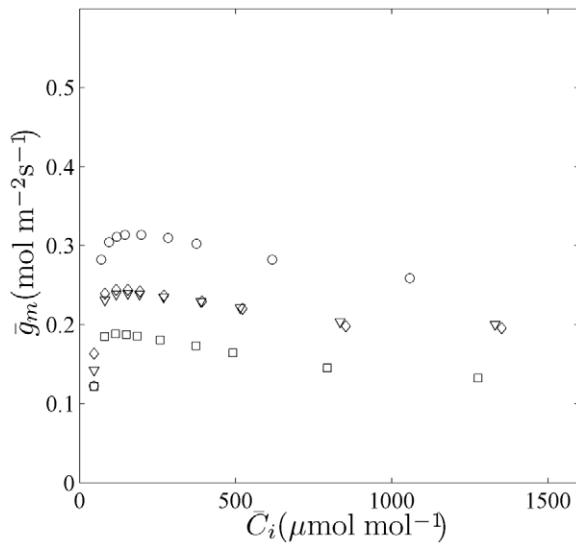
Figure 7. Model predictions of $\bar{g}_m$ as a function of $\overline{C_i}$ in high N supply flag leaves at flowering stage using four different microstructure topologies of wheat leaves. The simulations were done for different external CO_2 concentrations from 50 to 1500 µmol·mol⁻¹, $I_{inc} = 1000$ µmol m⁻² s⁻¹ in photorespiration conditions (21% O_2). Different symbols correspond to different microstructure topologies.
doi:10.1371/journal.pone.0048376.g007

Model of photosynthesis kinetics

The FvCB model was used in this article to describe the gross CO_2 fixation rate A_G in the chloroplasts of C_3 plants [16,29,67,68]. Briefly,

$$A_G = \left(1 - \frac{\Gamma *}{C_c}\right)\min\left(w_c, w_j, w_p\right) \qquad (1)$$

with w_c the Rubisco-limited carboxylation rate, w_j the RuBP-regeneration or electron transport limited rate, and w_p the triose phosphate utilization (TPU) limited rate. They were calculated from

$$w_c = \frac{C_c \cdot V_{c,max}}{C_c + K_{m,C}(1 + O_2/K_{m,O_2})} \qquad (2)$$

$$w_j = \frac{C_c \cdot J}{4C_c + 8\Gamma *} \qquad (3)$$

$$w_p = \frac{3T_p}{\left(1 - \frac{\Gamma *}{C_c}\right)} \qquad (4)$$

with C_c and O_2 the CO_2 and O_2 concentration in the chloroplast, respectively; J the rate of electron transport; T_p the rate of triose phosphate export from the chloroplast; and $\Gamma * = 0.5 O_2/S_{c/o}$ [17]. $K_{m,C}$, K_{m,O_2} and $V_{c,max}$ are constants. The meaning and units of all symbols are given in Table 1. The net photosynthesis rate A was defined as $A = A_G - R_d$, with R_d the respiratory CO_2 release other than by photorespiration.

Microscale gas exchange model

The exchange of CO_2 in the tissue was described by means of a reaction diffusion equation:

$$\frac{\partial C}{\partial t} = \nabla \cdot D \nabla C - A_G^* + R_d^* + B \qquad (5)$$

$$\frac{\partial C_{HCO_3^-}}{\partial t} = \nabla \cdot D_{HCO_3^-} \nabla C_{HCO_3^-} - B \qquad (6)$$

with C and $C_{HCO_3^-}$ the local CO_2 and HCO_3^- concentration; D and $D_{HCO_3^-}$ the corresponding local diffusivity coefficients; and t time. The volumetric photosynthesis rate A_G^* was assumed to be equal to zero everywhere except in the chloroplasts. A_G^* and R_d^* were calculated from A_G and R_d using

$$A_G^* = A_G/(d \cdot f_c) \qquad (7)$$

$$R_d^* = R_d/(d \cdot f_m) \qquad (8)$$

with d (184 µm) the average thickness of the leaf, and f_c (0.104) and f_m (0.169) the fraction of chloroplasts and cytosol in a 2-D cross section of the leaf, respectively. B represents the net hydration rate of CO_2 to HCO_3^-:

$$B = k_2 \frac{[H]^+ C_{HCO_3^-,c}}{K} - k_1 C_c \qquad (9)$$

The CO_2 flux ϕ through the membranes of the cell, chloroplast and vacuole membranes was described by a flux boundary condition:

$$\phi = -P_m \Delta C \qquad (10)$$

with P_m the membrane permeability that is equal to the reciprocal of resistance. It was assumed that the local CO_2 concentration in the gas and liquid phase was always in equilibrium and described by Henry's law.

Geometrical model

The 2-D geometry of wheat leaf was constructed from light microscopic images of wheat leaf available from the literature [35], as the experimental dataset of Yin et al. [17] did not contain microscopic images. As the leaf cross section consists of several similar parallel vein segments, only one segment was modelled and impermeable boundary conditions were applied at the left and right hand side of the geometrical model. The images were digitized in the Matlab programming environment version 7.0 (The Mathworks, Natick, MA) by in-house developed software (Figure 8). The cells were represented by polygons. The bottom and top cell layers constituted the epidermis. The thickness of plant cell walls generally lies in the range of 0.1 to 0.3 µm, but can exceed 1 µm [69,70]. As it was not possible to determine the cell wall thickness accurately from the light microscopic images, we constructed the cell wall by shrinking the original polygon representing a cell by 0.5 µm normal to every edge; the volume between the original and shrunk polygon was defined as the cell wall. Since the model was solved using the finite element method, reducing the cell wall thickness would decrease the mesh size in the
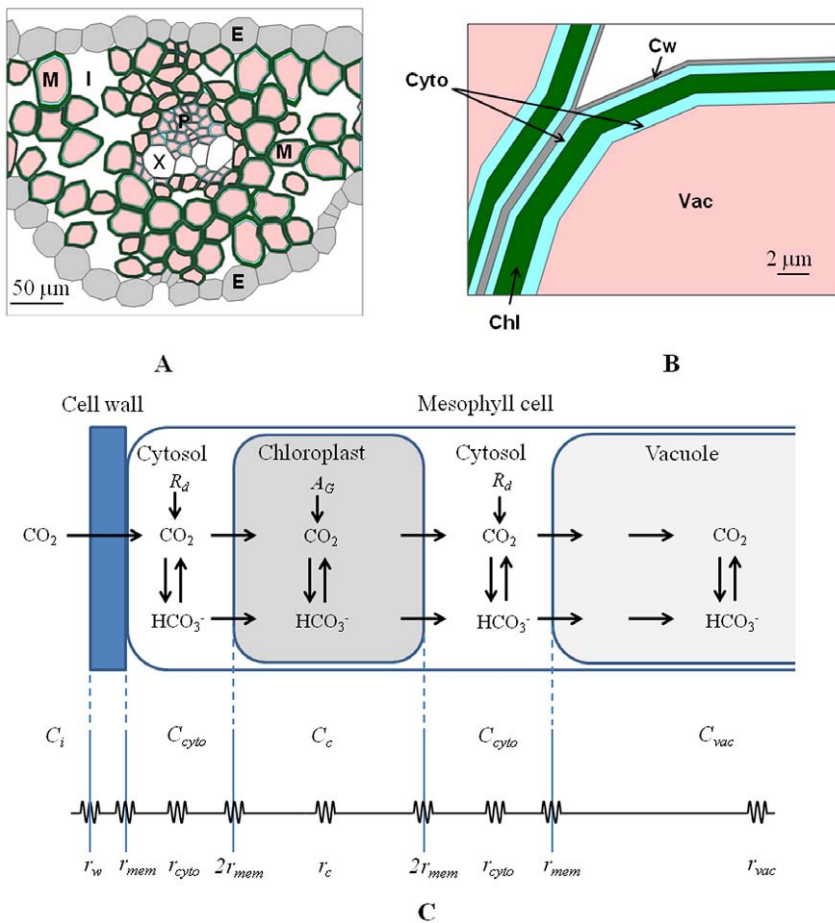
Figure 8. Reconstructed microscale geometry based on microscopic images of wheat leaf tissue and scheme of fluxes of CO₂ species through different compartments of the mesophyll cell. (A) Reconstructed microscale geometry based on microscopic images of wheat leaf tissue [35]. The adaxial surface is at the bottom. E, epidermis; I, intercellular space; M, mesophyll cell; P, phloem; and X, xylem. (B) Detail of reconstructed mesophyll cells in computer model. Chl, chloroplast layer; Cyto, cytoplasm; Cw, cell wall; Vac, vacuole.(C) Scheme of fluxes of CO₂ species through different compartments of the mesophyll cell and corresponding resistances. The resistances due to the epidermis, stomata and intercellular space are not included in this scheme. The symbols C and r indicate CO₂concentration and resistance, respectively. The subscripts i, w, $cyto$, c, vac and mem indicate intercellular space, cell wall, cytoplasm, chloroplast, vacuole and membrane, respectively. The resistance of double membrane- chloroplast envelope was modeled as twice the resistance of the phospholipid membrane. A_G is the gross photosynthesis rate; R_d is respiration.
doi:10.1371/journal.pone.0048376.g008

cell wall material and, hence, increase the required computational resources and time. This would not affect the model predictions appreciably as the cell wall thickness is interchangeable with D_w: if we would have implemented a smaller cell wall thickness the parameter estimation procedure would have resulted in a larger value of D_w, but the simulation results would be virtually identical. Chloroplasts appear as flat discs usually 2 to 10 μm in diameter and 1 μm thick. A mesophyll cell can contain 10 to 100 chloroplasts [71]. James et al. [72] found that the volume fraction of chloroplasts in the mesophyll cells was about 24%. For simplicity, chloroplasts were modeled as a layer located at a distance of 0.5 μm from the cell wall and occupying 20% of the modelled mesophyll cell volume. The relative photosynthetic capacity $V_{c,max}(y)$ at a well defined depth y inside the leaf was calculated as

$$V_{c,max}(y) = \int_{w(y),x\in chloroplast} dx / (f_c . \int_{w(y)} dx) \qquad (11)$$

where the integration is over the width $w(y)$ of the leaf at the depth y. The distribution of photosynthesis capacity $V_{c,max}(y)$ along the depth of the leaf depends on distribution of chlorophyll through the leaf, the presence of vascular region (Figure 2). The vacuolar volume fraction is variable and can be larger than 30% of the cell volume and up to 90% of the cell volume in a mature cell [71]. The vacuoles were modelled explicitly in the mesophyll cells by shrinking the cell area of 2D geometry by 60% and considering the shrunk area to be vacuole. For a spherical cell, for example, this corresponds to a vacuolar volume fraction of 46%. The layer between the cell membrane and the chlorophyll layer and that between the tonoplast and the chlorophyll layer was considered to be cytoplasm. This implies that CO₂ to reach the vacuole has to pass the cell wall, the plasmalemma, twice the chloroplast membrane, and finally the tonoplast. In reality CO₂ can diffuse directly from the plasmalemma to the tonoplast, but we believe that ignoring this only marginally affects intercellular CO₂ transport while it simplifies the geometrical model considerably.

The resulting geometry of the tissue was then exported into a finite element simulation code (Comsol 3.5, Comsol AB, Stock-

holm, Sweden) via a Matlab interface. The leaf geometry and the corresponding finite element mesh that was used for the simulations are shown in Figure 8.

Gas exchange and chlorophyll fluorescence measurements

Data used for our analysis came from measurements reported by Yin et al. [17] for photosynthesis of wheat plants grown under two contrasting levels of nitrogen supply. Nutrient supply is known to enhance photosynthesis, whereas it has a rather small and inconsistent effect on g_m [73]. Simultaneous gas exchange and chlorophyll fluorescence measurements at both 21% and 2% O_2 were performed on main-stem flag leaves at the flowering stage and two weeks after flowering, with four replications at each stage, using an open gas exchange system (Li-Cor 6400; Li-Cor Inc, Lincoln, NE, USA) and an integrated fluorescence chamber head (LI-6400-40; Li-Cor Inc, Lincoln, NE, USA). All measurements were made at a leaf temperature (T_{leaf}) of 25°C and a leaf-to-air vapour pressure difference of 1.0–1.6 kPa. For the C_i response curves, the ambient air CO_2 concentration (C_a) was increased step-wise: 50, 100, 150, 200, 250, 350, 500, 650, 1000, and 1500 μmol mol^{-1}, while keeping incident irradiance I_{inc} at 1000 μmol m^{-2} s^{-1}. For the I_{inc} response curves, the photon flux densities were in a series: 0, 20, 50, 100, 150, 200, 500, 1000, 1500, 2000 μmol m^{-2} s^{-1}, while keeping C_a at 350 μmol mol^{-1} for measurements at 21% O_2, and keeping C_a at 1000 μmol mol^{-1} for measurements at 2% O_2 to ensure a non-photorespiration condition. The photosynthetic parameters of the FvCB model were estimated from these measurements [17] and are given in Table 4.

Definition of macroscale variables

The microscale model predicts local variables which may depend on the position inside the leaf, whereas the gas exchange and chlorophyll fluorescence experiments measure lumped, macroscale variables of the whole leaf. In order to compare both measurements and simulations, equivalent macroscale variables need to be calculated from the microscale simulation results. We will use the following convention for symbols: macroscopic variables which were estimated from gas exchange and chlorophyll fluorescence experiments are denoted by a '∧' symbol. Volume averaged variables (area averaged variables in the 2-D model) calculated from the microscale model are overlined.

Chlorophyll fluorescence measurements can assess the photosystem II (PSII) electron transport efficiency as $\Delta F/F'_m = (F'_m - F_s)/F'_m$, where F_s is the steady-state fluorescence, F'_m is the maximum fluorescence during a saturating light pulse [74]. Data for $\Delta F/F'_m$ can be converted into the flux of potential electron transport ($\hat{J}$) according to

$$J = sI_{inc}\Delta F/F'_m \qquad (12)$$

where s is a calibration factor that can be estimated as the slope of the empirical linear relation between A and $I_{inc}(\Delta F/F'_m)/4$ using data of non-photorespiratory measurements at 2% O_2 combined with high CO_2 levels (see Yin et al. [17], for more details). Using $\hat{J}$ estimated from the chlorophyll fluorescence measurements under photorespiration conditions, the mean mesophyll CO_2 concentration $\hat{C}_c$ was estimated as [10]:

Table 4. Values (± standard error of estimate if applicable) of photosynthetic parameters estimated for flag leaves of wheat plants at flowering grown at low nitrogen (N) and high N levels at flowering stage. Estimates were made separately for photorespiratory (PR) and non-photorespiratory (NPR) conditions when necessary [17].

Parameters	High N	Low N
$V_{c,max}$ (μmol m^{-2} s^{-1})	65.8±0.8	58.5±0.8
$K_{m,C}$ (μbar)	168±17	168±17
K_{m,O_2} (mbar)	473	473
$S_{c/o}$ (mbar μbar^{-1})	3.13	3.13
s	0.380	0.403
Γ^* (μbar)	34	34
R_d (μmol m^{-2} s^{-1}) PR	1.317	0.939
R_d (μmol m^{-2} s^{-1}) NPR	1.573	1.375
T_p (μmol m^{-2} s^{-1})	12.9±0.13	11.1±0.19

doi:10.1371/journal.pone.0048376.t004

$$\hat{C}_c = \frac{\Gamma^*[J/4 + 2(\hat{A}+R_d)]}{J/4 - (\hat{A}+R_d)} \qquad (13)$$

where $\hat{A}$ is the net CO_2 assimilation rate based on the gas exchange measurements.

The volume averaged CO_2 concentration of the mesophyll cell ($\overline{C}_c$) predicted by the microscale model was computed as

$$\overline{C}_c = \frac{\int_{V_m} C_c dV}{\int_{V_m} dV} = \frac{\int_{V_m} C_c dV}{V_m} \qquad (14)$$

The integration domain V_m in Equation (14) is the volume (area in 2-D) of all mesophyll cells in the 2-D microstructural image of the leaf tissue.

On the basis of the assumption that C_c can be reliably estimated by Equation (13) from combined gas exchange and chlorophyll fluorescence data, the mesophyll conductance $\hat{g}_m$ was calculated from [10]:

$$\hat{g}_m = \frac{\hat{A}}{\hat{C}_i - \hat{C}_c} = \frac{\hat{A}}{\hat{C}_i - \frac{\Gamma^*[J/4 + 2(\hat{A}+R_d)]}{J/4 - (\hat{A}+R_d)}} \qquad (15)$$

where $\hat{C}_i$ is the intercellular CO_2 concentration from gas exchange measurements [7] and $\hat{A}$ the measured photosynthesis rate. The equivalent whole-leaf $\overline{g}_m$ predicted by the microscale model is

$$\overline{g}_m = \frac{\overline{A}}{\overline{C}_i - \overline{C}_c} \qquad (16)$$

where $\overline{C}_i$ is the volume averaged intercellular CO_2 concentration and computed from the microscale model according to a similar expression as in Equation (14). The whole leaf photosynthesis rate $\overline{A}$ is calculated by integrating the CO_2 flux from the epidermis to the ambient over the entire exchange surface.

Table 5. Description of data sets used in calibration and validation of model.

	Data set	Nitrogen (N) supply	Development stage	[CO$_2$] (μmol mol^{-1})	I_{inc} (μmol m^{-2} s^{-1})	O$_2$ (%)	Experiments
Calibration	A1	High N	Flowering stage	350	1000	21	CO$_2$ response curves
	A2	High N	Flowering stage	350	0, 20, 50, 100, 150, 200, 500, 1000, 1500, 2000	21	I_{inc} response curves
Validation	A1	High N	Flowering stage	50, 100, 150, 200, 250, 500, 650, 1000, 1500	1000	2, 21	CO$_2$ response curves
	B1	Low N	Flowering stage	50, 100, 150, 200, 250, 350, 500, 650, 1000, 1500	1000	2, 21	CO$_2$ response curves
	C1	High N	2 weeks after flowering	50, 100, 150, 200, 250, 350, 500, 650, 1000, 1500	1000	2, 21	CO$_2$ response curves
	D1	Low N	2 weeks after flowering	50, 100, 150, 200, 250, 350, 500, 650, 1000, 1500	1000	2, 21	CO$_2$ response curves
	B2	Low N	Flowering stage	350	0, 20, 50, 100, 150, 200, 500, 1000, 1500, 2000	21	I_{inc} response curves
	C2	High N	2 weeks after flowering	350	0, 20, 50, 100, 150, 200, 500, 1000, 1500, 2000	21	I_{inc} response curves
	D2	Low N	2 weeks after flowering	350	0, 20, 50, 100, 150, 200, 500, 1000, 1500, 2000	21	I_{inc} response curves

doi:10.1371/journal.pone.0048376.t005

Model calibration and validation

The model equations were solved using the finite element environment Comsol Multiphysics vs. 3.5 (Comsol AB, Stockholm). The non-linear coupled model equations from (1) to (10) were discretized over the finite element mesh using the weak formulation [75]. The model equations were solved for steady-state conditions. Between the organelles, permeation through the membranes was taken into account. A direct solver was used for solving the resulting set of ordinary differential equations with relative tolerance less than 10^{-6}.

Gas transport properties were obtained from the literature (Table 3). The photosynthetic parameters of the FvCB model for different N treatments and life stages were obtained from Yin et al.[17]. $V_{c,max}$ was estimated based on the chloroplastic CO$_2$ concentration. The potential electron transport rate J was calculated from the chlorophyll fluorescence measurements (Equation 12). We assumed that all membranes had the same permeability (value indicated in Table 3), but because the chloroplast envelope is a double membrane we assigned half the permeability of the other (single) membranes to it.

For model calibration, data from experiments A1 and A2 of Table 5 were used. Using the photosynthesis response to ambient CO$_2$ concentration (Yin et al. [17]), the diffusivity values of the epidermis (D_{epi}) and of the cell wall (D_w) were estimated simultaneously by fitting the calculated CO$_2$ concentration of the intercellular space and the mesophyll CO$_2$ concentration determined from microscale model to the experimental data using a nonlinear least square estimation procedure in Matlab (The Mathworks, Inc., Natick, USA). The boundary condition used in the parameter estimation was 350 μmol mol^{-1} CO$_2$ at 21% O$_2$ while keeping I_{inc} at 1000 μmol m^{-2} s^{-1} and T_{leaf} at 25°C. The resulting values were equal to 1.67×10^{-7} m^2 s^{-1} and 3.437×10^{-7} m^2 s^{-1} for D_{epi} and D_w, respectively (Table 3). Note that for reasons outlined before the stomata were not modelled explicitly but their conductance was implicitly included in D_{epi}. Irradiation affects stomatal aperture [34] and a significant effect on the measured stomatal conductance has been observed. Thus, for modelling of photosynthesis in response to irradiation, D_{epi} can be expected to vary with irradiance. For each measured light intensity, the corresponding D_{epi} was therefore determined by fitting $\bar{g}_s$ to $\hat{g}_s$ while keeping D_w at the value determined previously.

For validation, the model predictions were compared to experimental data that were not used for the parameter estimation, i.e. dataset B1, C1, D1, B2, C2 and D2 of Table 5. The same values of D_{epi} and D_w as in the calibration experiments were assumed.

Supporting Information

Text S1 Lumped microscale modeling.
(DOC)

Figure S1 Computed CO$_2$ distribution in wheat leaf according to the model with and without chloroplasts. The ambient conditions were 350 μmol mol^{-1} CO$_2$, 21% O$_2$, $I_{inc} = 1000$ μmol m^{-2} s^{-1} and $T_{leaf} = 25$°C. Concentrations are expressed in μmol m^{-3}. (A) and (B) are simulation results with and without chloroplasts.
(TIF)

Figure S2 Simulations and measurements at different conditions of C_i at 21% O$_2$, $I_{inc} = 1000$ μmol m^{-2} s^{-1} and 25°C. The left and right figures represent simulations at two weeks after flowering for high and low N supply flag leaves,

respectively. Figures (A) and (B) show the net CO_2 assimilation rate (A) as function of intercellular CO_2 concentration C_i. The symbols represent measurements ($\hat{A}$ versus $\widehat{C_i}$) while the lines indicate model predictions ($\overline{A}$ versus $\overline{C_i}$). Figures (C) and (D) depict $\hat{C_c}$ versus $\overline{C_c}$. The diagonal lines indicate perfect correspondence. Figures (E) and (F) show g_m as function of C_i. The solid (—) line represents $\overline{g}_m$ versus $\overline{C_i}$. The symbols (o) represent the measured data ($\hat{g}_m$ versus $\widehat{C_i}$). Data are from Yin et al. [17].
(TIF)

Figure S3 Model predictions (lines) versus measurements (symbols) of photosynthesis variables for 350 μmol mol^{-1} CO_2, 21% O_2, I_{inc} from 0 to 2000 μmol m^{-2} s^{-1} and 25°C. Left figures and right figures represent simulations for high N and low N supply flag leaves at two weeks after flowering. Figure (A) and (B) show C_i and C_c as function of I_{inc}; the solid lines (—) and dashed lines (- -) represent $\overline{C_i}$ and $\overline{C_c}$, symbols (×) and (o) represent $\widehat{C_i}$ and $\widehat{C_c}$, respectively. Figure (C) and (D) show A as function of I_{inc}, while figure (E) and (F) indicate the mesophyll conductance $\overline{g}_m$ (—) or $\hat{g}_m$ (o) as function of I_{inc}. Data from Yin et al. [17].
(TIF)

Figure S4 Simulated net photosynthesis of wheat leaf as function of temperature. (A) Temperature dependence of $V_{c,max}$ and J_{max}. Values are normalized to 1 at 25°C. Arrhenius-like

expressions for $V_{c,max}$ and J_{max} as a function of temperature are described by [44] and [29], respectively. (B) Simulated net photosynthesis of wheat leaf as function of temperature. $\overline{A}$, $\overline{A}_c$ and $\overline{A}_j$ are the mean net photosynthesis rate, rubisco activity limited net photosynthesis rate and electron transport limited net photosynthesis rate computed from the microscale model. $V_{c,max}$ and J_{max} as function of temperature are taken from [44] and [29], respectively while the temperature dependence of other FvCB parameters (R_d, Γ^*, $K_{m,C}$, K_{m,O_2}) were was from [39] and [40]. Model predictions of photosynthesis were for high N wheat leaf at the flowering stage, 350 μmol mol^{-1} CO_2, 21% O_2, I_{inc} of 1000 μmol m^{-2} s^{-1}.
(TIF)

Author Contributions

Conceived and designed the experiments: BMN QTH PV XY PCS. Performed the experiments: XY PCS. Analyzed the data: QTH PV BMN. Contributed reagents/materials/analysis tools: BMN QTH PV XY PCS. Wrote the paper: BMN QTH PV XY PCS.

References

1. Flexas J, Diaz-Espejo A, Galmes J, Kaldenhoff R, Medrano H, et al. (2007) Rapid variation of mesophyll conductance in response to changes in CO_2 concentration around leaves. Plant Cell Environ 30: 1284–1298.
2. Flexas J, Ribas-Carbó M, Diaz-Espejo A, Galmes J, Medrano H (2008) Mesophyll conductance to CO_2: current knowledge and future prospects. Plant Cell Environ 31:602–621.
3. Tholen D, Zhu X-G (2011) The mechanistic basis of internal conductance: a theoretical analysis of mesophyll cell photosynthesis and CO_2 diffusion. Plant Physiol 156:90–105.
4. Farquhar GD, Sharkey TD (1982) Stomatal conductance and photosynthesis. Ann Rev Plant Physiol 33:317–345.
5. Bernacchi CJ, Portis AR, Nakano H, von Caemmerer S, Long SP (2002) Temperature response of mesophyll conductance. Implication for the determination of Rubisco enzyme kinetics and for limitations to photosynthesis in vivo. Plant Physiol 130: 1992–1998.
6. Goudriaan J, van Laar HH (1978) Relations between resistance, CO_2 concentration and CO_2 assimilation in maize, beans, lalang grass and sunflower. Photosynthetica 12: 241–249.
7. von Caemmerer S, Farquhar GD (1981) Some relationships between the biochemistry of photosynthesis and the gas-exchange of leaves. Planta 153: 376–387.
8. Bongi G, Loreto F (1989) Gas-exchange properties of salted-stressed olive (*Olea europea* L.) leaves. Plant Physiol 90: 1408–1416.
9. Di Marco G, Manes F, Tricoli D, Vitale E (1990) Fluorescence parameters measured concurrently with net photosynthesis to investigate chloroplastic CO_2 concentration in leaves of Quercus ilex L. J Plant Physiol 136: 538–543.
10. Harley PC, Loreto F, Di Marco G, Sharkey TD (1992) Theoretical considerations when estimating the mesophyll conductance to CO_2 flux by analysis of the response of photosynthesis to CO_2. Plant Physiol 98: 1429–1436.
11. Evans JR, von Caemmerer S (1996) Carbon dioxide diffusion inside leaves. Plant Physiol 110: 339–346.
12. Yin X, Struik PC (2009) Theoretical reconsiderations when estimating the mesophyll conductance to CO_2 diffusion in leaves of C_3 plants by analysis of combined gas exchange and chlorophyll fluorescence measurements. Plant Cell Environ 32: 1513–1524 (corrigendum in Plant Cell Environ 33: 1595).
13. Loreto F, Harley PC, Di Marco G, Sharkey TD (1992) Estimation of mesophyll conductance to CO_2 flux by three different methods. Plant Physiol 98: 1437–1443.
14. Evans JR, von Caemmerer S, Setchell BA, Hudson GS (1994) The relationship between CO_2 transfer conductance and leaf anatomy in transgenic tobacco with a reduced content of Rubisco. Aust J Plant Physiol 21: 475–495.
15. von Caemmerer S, Evans JR, Hudson GS, Andrews TJ (1994) The kinetics of ribulose-1,5-bisphosphate carboxylase/oxygenase in vivo inferred from measurements of photosynthesis in leaves of transgenic tobacco. Planta 195: 88–97.
16. von Caemmerer S (2000) Biochemical models of leaf photosynthesis. In: Techniques in Plant Sciences No. 2. Collingwood, Victoria, Australia: CSIRO Publishing. p.196.
17. Yin X, Struik PC, Romero P, Harbinson J, Evers JB, et al. (2009) Using combined measurements of gas exchange and chlorophyll fluorescence to estimate parameters of a biochemical C-3 photosynthesis model: a critical appraisal and a new integrated approach applied to leaves in a wheat (*Triticum aestivum*) canopy. Plant Cell Environ 32: 448–464.
18. von Caemmerer S, Evans JR (1991) Determination of the average partial pressure of CO_2 in chloroplasts from leaves of several C_3 plants. Aust J Plant Physiol 18: 287–305.
19. Centritto M, Loreto F, Chartzoulakis K (2003) The use of low [CO2] to estimate diffusional and non-diffusional limitations of photosynthetic capacity of salted-stressed olive saplings. Plant Cell Environ 26: 585–594.
20. Evans JR, Kaldenhoff R, Genty B, Terashima I (2009) Resistances along the CO_2 diffusion pathway inside leaves. J Exp Bot 60: 2235–2248.
21. Tholen D, Boom C, Noguchi K, Ueda S, Katase T, et al. (2008) The chloroplast avoidance response decreases internal conductance to CO_2 diffusion in *Arabidopsis thaliana* leaves. Plant Cell Environ 31: 1688–1700.
22. Terashima I, Hanba YT, Tholen D, Niinemets U (2011) Leaf functional anatomy in relation to photosynthesis. Plant Physiol 155: 108–116.
23. Vesala T, Ahonen T, Hari P, Krissinel E, Shokhirev N (1996) Analysis of stomatal CO_2 uptake by a three-dimensional cylindrically symmetric model. New Phytol 132: 235–245.
24. Aalto T, Juurola E (2002) A three-dimensional model of CO_2 transport in airspaces and mesophyll cells of a silver birch leaf. Plant Cell Environ 25:1399–1409.
25. Uehlein N, Otto B, Hanson DT, Fischer M, McDowell N, et al. (2008) Function of *Nicotiana tabacum* aquaporins as chloroplast gas pores challenges the concept of membrane CO2 permeability. Plant Cell 20: 648–657.
26. Ho QT, Verboven P, Mebatsion HK, Verlinden BE, Vandewalle S, et al. (2009) Microscale mechanisms of gas exchange in fruit tissue. New Phytol 182: 163–174.
27. Ho QT, Verboven P, Verlinden BE, Herremans E, Wevers M, et al. (2011) A 3-D multiscale model for gas exchange in fruit. Plant Physiol 155: 1158–1168.
28. Ho QT, Verboven P, Verlinden BE, Nicolaï BM (2010) A model for gas transport in pear fruit at multiple scales. J Exp Bot 61: 2071–2081.
29. Farquhar GD, von Caemmerer S, Berry JA (1980) A biochemical model of photosynthetic CO_2 assimilation in leaves of C_3 species. Planta 149: 78–90.
30. Leuning R (1995) A critical appraisal of a combined stomatal-photosynthesis model for C_3 plant. Plant Cell Environ 18: 339–355.
31. Kim SH, Heinrich Lieth J (2003) A coupled model of photosynthesis, stomatal conductance and transpiration for rose leaf (*Rosa hybrida* L.). Ann Botany 91: 771–781.

32. Sharkey TD, Bernachhi CJ, Farquhar GD, Singsaas EL (2007) Fitting photosynthetic carbon dioxide response curves for C$_3$ leaves. Plant Cell Environ 30: 1035–1040.
33. Yin X, Struik PC (2009) C$_3$ and C$_4$ photosynthesis models: An overview from the perspective of crop modelling. NJAS-Wageningen Journal of Life Sciences 57: 27–38.
34. Morison JIL, Jarvis PG (1983) Direct and indirect effects of light on stomata. Plant Cell Environ 6: 103–109.
35. Hu Y, Fromm J, Schmidhalter U (2005) Effect of salinity on tissue architecture in expanding wheat leaves. Planta 220: 838–848.
36. Parkhurst DF (1994) Diffusion of CO$_2$ and other gases inside leaves. New Phytol 126:449–479.
37. Farquhar GD, von Caemmerer S (1982) Modelling of photosynthetic response to environmental conditions. In: Lange OL, Nobel PS, Osmond CB, Ziegler H, editors. Physiological Plant Ecology II. Water relations and carbon assimilation. Encyclopedia of Plant Physiol. New Series, Vol. 12 B. Berlin: Springer. pp. 549–588.
38. Parkhurst DF, Mott KA (1990) Intercellular diffusion limits to CO$_2$ uptake in leaves. Studies in air and helox. Plant Physiol 94:1024–1032.
39. Dreyer E, Le Roux X, Montpied P, Daudet AF, Masson F (2001) Temperature response of leaf photosynthetic capacity in seedlings from seven temperate tree species. Tree Physiol 21:223–232.
40. Medlyn BE, Dreyer E, Ellsworth D, Forstreuter M, Harley PC, et al. (2002). Temperature response of parameters of a biochemically based model of photosynthesis. II. A review of experimental data. Plant Cell Environ 25:1167–1179.
41. Archontoulis SV, Yin X, Vos J, Danalatos NG, Struik PC (2012). Leaf photosynthesis and respiration of three bioenergy crops in relation to temperature and leaf nitrogen: how conserved are biochemical model parameters among crop species?. J Exp Bot 63:895–911.
42. De Pury DGG, Farquhar GD (1997) Simple scaling of photosynthesis from leaves to canopies without the errors of the big-leaf models. Plant Cell Environ 20:537–557.
43. Lide DR (1999) In:Handbook of Chemistry and Physics. Boca Raton: CRC Press.
44. Badger MR, Collatz GJ (1977) Studies on the kinetic mechanism of ribulose-1,5-bisphosphate carboxylase and oxygenase reactions, with particular reference to the effect of temperature on kinetic parameters. Carnegie Institute of Washington Yearbook 16: 355–361.
45. Gillon JS, Yakir D (2000) Internal conductance to CO$_2$ diffusion and C^{18}OO discrimination in C$_3$ leaves. Plant Physiol 123: 201–213.
46. Fabre N, Reiter IM, Becuwe-Linka N, Genty B, Rumeau D (2007) Characterization and expression analysis of genes encoding a and b carbonic anhydrases in *Arabidopsis*. Plant Cell Environ 30: 617–629.
47. Gutknecht J, Bisson MA, Tosteson FC (1977) Diffusion of carbon dioxide through lipid bilayer membranes: effect of carbonic anhydrase, bicarbonate, and unstirred layers. J Gen Physiol 69: 779–794.
48. Evans JR, Loreto F (2000) Acquisition and diffusion of CO$_2$ in higher plant leaves. In: Leegood RC, Sharkey TD, von Caemmerer S, editors. Photosynthesis: Physiology and Metabolism. Dordrecht, The Netherlands: Kluwer Academic Publishers. pp. 321–351.
49. Terashima I, Hanba YT, Tazoe Y, Vyas P, Yano S (2006) Irradiance and phenotype: comparative eco-development of sun and shade leaves in relation to photosynthetic CO$_2$ diffusion. J Exp Bot 57: 343–354.
50. Evans JR, Vogelmann TC (2003) Profiles of ^{14}C fixation through spinach leaves in relation to light absorption and photosynthetic capacity. Plant Cell Environ 26:547–560.
51. Evans JR, Vogelmann TC (2006) Photosynthesis within isobilateral Eucalyptus pauciflora leaves. New Phytol 171: 771–782.
52. Colman B, Espie GS (1985) CO$_2$ uptake and transport in leaf mesophyll cells. Plant Cell Environ 8: 449–457.
53. Lloyd J, Syvertsen JP, Kriedemann PE, Farquhar GD (1992) Low conductances for CO$_2$ diffusion from stomata to the sites of carboxylation in leaves of woody species. Plant Cell Environ 15: 873–899.
54. Syvertsen JP, Lloyd J, McConchie C, Kriedemann PE, Farquhar GD (1995) On the relationship between leaf anatomy and CO$_2$ diffusion through the mesophyll of hypostomatous leaves. Plant Cell Environ 18: 149–157.
55. Pieruschka R, Schurr U, Jahnke S (2005) Lateral gas diffusion inside leaves. J Exp Bot 56: 857–864.
56. Morison JIL, Gallouet E, Lawson T, Cornic G, Herbin R, et al. (2005) Lateral diffusion of CO$_2$ in leaves is not sufficient to support photosynthesis. Plant Physiol 139: 254–266.
57. Morison JIL, Lawson T, Cornic G (2007) Lateral CO$_2$ diffusion inside dicotyledonous leaves can be substantial: quantification in different light intensities. Plant Physiol 145: 680–690.
58. Kuroki S, Oshita S, Sotome I, Kawagoe Y, Seo Y (2004) Visualisation of 3-D network of gas-filled intercellular spaces in cucumber fruit after harvest. Postharvest Biol Technol 33: 255–262.
59. Mendoza F, Verboven P, Mebatsion HK, Kerckhofs G, Wevers M, et al. (2007) Three-dimensional pore space quantification of apple tissue using X-ray computed microtomography. Planta 226: 559–570.
60. Verboven P, Kerckhofs G, Mebatsion HK, Ho QT, Temst K, et al. (2008) 3-D gas exchange pathways in pome fruit characterised by synchrotron X-ray computed tomography. Plant Physiol 147: 518–527.
61. Kaiser H (2009) The relation between stomatal aperture and gas exchange under consideration of pore geometry and diffusional resistance in the mesophyll. Plant Cell Environ 32: 1091–1098.
62. Evans JR (2009) Potential errors in electron transport rates calculated from chlorophyll fluorescence as revealed by a multilayer leaf model. Plant and Cell Physiol 50: 698–706.
63. Terashima I, Fujita T, Inoue T, Chow WS, Oguchi R (2009) Green light drives leaf photosynthesis more efficiently than red light in strong white light: revisiting the enigmatic question of why leaves are green. Plant and Cell Physiol 50: 684–697.
64. Verboven P, Pedersen O, Herremans E, Ho QT, Nicolaï BM, et al. (2011) Root aeration via aerenchymatous phellem – 3-D micro-imaging and radial O$_2$ profiles in *Melilotus siculus*. New Phytol 193: 420–431.
65. Terashima I, Saeki T (1985) A new model for leaf photosynthesis incorporating the gradients of light environment and of photosynthetic properties of chloroplasts within a leaf. Ann Bot 56: 489–499.
66. Vogelmann TC, Evans JR (2002) Profiles of light absorption and chlorophyll within spinach leaves from chlorophyll fluorescence. Plant Cell Environ 25: 1313–1323.
67. Sharkey TD (1985) Photosynthesis in intact leaves of C3 plants: physics, physiology and rate limitations. Bot Rev 51: 53–105.
68. Yin X, van Oijen M, Schapendonk AHCM (2004) Extension of a biochemical model for the generalised stoichiometry of electron transport limited C3 photosynthesis. Plant Cell Environ 27: 1211–1222.
69. Rezvani Moghaddam P, Wilman D (1998) Cell wall thickness and cell dimensions in plant parts of eight forage species. J Agric Sci 131: 59–67.
70. Dupuy L, Mackenzie J, Haseloff J (2010) Coordination of plant cell division and expansion in a simple morphogenetic system. PNAS 107: 2711–2716.
71. Buchanan BB, Gruissem W, Jones RL (2000) In:Biochemistry and molecular biology of plants. Rockville, Maryland: American Society of Plant Physiologists.
72. James RA, Munns R, von Caemmerer S, Trejo C, Miller C, et al. (2006) Photosynthetic capacity is related to the cellular and subcellular partitioning of Na$^+$, K$^+$ and Cl$^-$ in salt-affected barley and durum wheat. Plant Cell Environ 29: 2185–2197.
73. Warren CR (2004) The photosynthetic limitation posed by internal conductance to CO$_2$ movement is increased by nutrient supply. J Exp Bot 55:2313–232.
74. Genty B, Briantais J, Baker N (1989) The relationship between the quantum yield of photosynthetic electron transport and quenching of chlorophyll fluorescence. Biochim Biophys Acta 990: 87–92.
75. Knabner P, Angermann L (2003) In:Numerical methods for elliptic and parabolic partial differential equations. New York: Springer-Verlag.
76. Geers C, Gros G (2000) Carbon dioxide transport and carbonic anhydrase in blood and muscle. Physiol Rev 80: 681–715.
77. Jolly WL (1985) In:Modern inorganic chemistry. New York: McGraw-Hill.